Modeling and Characterization of Pulse Shape and Pulse Train Dynamics in Two-Section Passively Mode-Locked Quantum Dot Lasers

R. Raghunathan[1], J. K. Mee[1,2], M. T. Crowley[3], F. Grillot[4] , V. Kovanis[5], and L. F. Lester[1]
[1]Center for High Technology Materials, University of New Mexico, 1313 Goddard SE, Albuquerque, NM 87106, USA.
[2]Air Force Research Laboratory, 3550 Aberdeen Ave SE, Kirtland AFB, NM 87120, USA
[3]BinOptics Corporation, Ithaca, NY 14850, USA.
[4]Telecom Paristech, Ecole National Supérieure des Télécommunications, CNRS LTCI, 75634 Paris Cedex 13, France
[5]Air Force Research Laboratory, 2241 Avionics Circle, Wright -Patterson AFB, Dayton, OH 45433, USA
Tel : (505)-272-7800 Fax: (505)-272-7801, email: raghunat@unm.edu

ABSTRACT

A nonlinear delay differential equation model for passive mode-locking in semiconductor lasers, seeded with parameters extracted from the gain and loss spectra of a quantum dot laser, is employed to simulate and study the dynamical regimes of mode-locked operation of the device. The model parameter ranges corresponding to these regimes are then mapped to externally-controllable parameters such as gain current and absorber bias voltage. Using this approach, a map indicating the approximate regions corresponding to fundamental and harmonically mode locked operation is constructed as a function of gain current and absorber bias voltage. This is shown to be a highly useful method of getting a sense of the highest repetition rates achievable in principle with a simple, two-section device, and provides a guideline toward achieving higher repetition rates by simply adjusting external biasing conditions instantaneously while the device is in operation, as opposed to re-engineering the device with additional passive or saturable absorber sections. The general approach could potentially aid the development of numerical modeling techniques aimed at providing a systematic guideline geared toward developing microwave and RF photonic sources for THz applications.

Keywords: Quantum dot lasers, nonlinear dynamics, delay differential equation model, passive mode-locking, harmonic mode-locking, pulse characteristics.

1. INTRODUCTION

Quantum dot mode-locked lasers (QDMLLs) have generated considerable interest in recent years as promising sources of low energy, low jitter, stable pulse trains[1, 2] for precision applications such as high bit rate optical communications[3, 4] and clocking[5], where identical pulses with a regular shape are sought at a desired repetition rate. The typically stringent (and often competing) performance requirements for such applications include high repetition rates on the order of tens of GHz, peak powers on the order of a few Watts and sub-10 ps pulse widths, all while maintaining stable pulse quality over variable operating conditions. To this end, recent work in our group and others has shown that higher repetition rates can be achieved without compromising on the other performance metrics aforementioned by implementing techniques such as making the device reconfigurable[6] (wherein, the position of the saturable absorber is varied within the cavity) and harmonic mode-locking using the double-interval technique[7] (wherein two saturable absorber sections positioned at specific locations in a multi-section device are used to stimulate a specific higher order repetition rate).

*raghunat@unm.edu; Phone: (505) 272-7931; Fax: (505) 272-7801

A key motivating factor in the quest for such techniques are the limitations inherent to simple, two-section QDMLL devices, such as the highest fundamental repetition rate achievable being limited by the cavity length (which, in turn, is limited by the relatively low maximum attainable optical gain that is characteristic of QD structures). The standard approach toward the design, fabrication and characterization of such devices involves an extensive cycle of iterative design and testing, where the objective is to find a configuration(s) that is acceptable for the target application.

In order to make this procedure more streamlined and efficient, a robust predictive modeling capability is highly desirable, since such a tool will firstly enable experimentation guided by theoretical predictions, as opposed to a trial-and-error approach. Secondly, numerical simulations allow a detailed study of how the nonlinear dynamics of the output are impacted by a variation of the input parameters, information that is critical to achieving controllability over device performance.

To this end, this paper builds on our previous efforts to better understand the pulse characteristics and mode locking stability of passively mode-locked QDMLLs[8, 9], with the objective of going a step further in providing a predictive guideline toward achieving higher pulse repetition rates. In continuation of our previous work, a nonlinear delay differential equation model[10-12] seeded with parameters measured on an actual device[13] is used to simulate the output mode locking regimes as input parameters are varied. The model parameters corresponding to each regime are then mapped to externally controllable parameters, so that the regions of fundamental and harmonic mode locking can be represented as a function of parameters that can be varied instantaneously, while the device is in operation.

In so doing, we propose a scheme to interactively switch the device to a higher or lower output pulse repetition rate, using just the external (electrical) bias controls. The approach offers a viable technique to achieving variable pulse repetition rates, without the need to re-engineer the device with additional sections.

2. THEORETICAL BACKGROUND

The Delay Differential Equation (DDE) model due to Vladimirov and Turaev is derived from the standard coupled Partial Differential Equation (PDE) formalism, which describes the interaction of a slowly varying complex optical field with the carrier densities in the gain and absorber sections of a generic semiconductor laser[11, 12]:

$$\frac{dA(\tau)}{d\tau} = \gamma\sqrt{\kappa}\, e^{\left\{\frac{1}{2}(1-i\alpha_g)G(\tau-T)-\frac{1}{2}(1-i\alpha_q)Q(\tau-T)\right\}} A(\tau-T) - \gamma A(\tau) \tag{1}$$

$$\frac{dG(\tau)}{d\tau} = g_0 - \Gamma G(\tau) - e^{-Q(\tau)}\left(e^{G(\tau)}-1\right)|A(\tau)|^2 \tag{2}$$

$$\frac{dQ(\tau)}{d\tau} = q_0 - Q(\tau) - s\left(1-e^{-Q(\tau)}\right)|A(\tau)|^2 \tag{3}$$

In equations (1)–(3) above, γ incorporates the effect of spectral filtering, α_g and α_q are the linewidth enhancement factors in the gain and absorber media respectively, and κ accounts for linear cavity losses. The delay parameter incorporates history, which appears in the first equation of the model through the evaluation of optical field A, saturable gain G, and saturable loss Q at the times $\tau - T$, where T denotes the normalized round trip time. Parameter $\Gamma = \left(\tau_{abs}/\tau_{gain}\right)$ is the ratio between the absorber and gain relaxation times, and s is the saturation parameter. Finally, g_0 and q_0 are the unsaturated gain and absorption, respectively.

In a recent experiment[9] performed by our group, it was shown that the segmented contact method[14, 15] can be used to obtain modal gain and total loss spectra as a function of gain current density, absorber bias voltage and temperature for the QD material comprising the device. These curves were used to extract the modal gain (g_{mod}) and unsaturated absorption (a_0) as a function of current density at each absorber bias condition. In the following, a systematic method to transform physically measured parameters from the gain and loss spectra into seed conditions for the DDE model is discussed.

The threshold condition for lasing can be expressed from equation (2) in [9] as follows:

$$\left(g_{\mathrm{mod}}(J)-\alpha_i\right)L_g - \left(a_0+\alpha_i\right)L_a = \alpha_m\left(L_a+L_g\right) \tag{4}$$

where, α_m and α_i represent, respectively, mirror losses and internal losses, and L_g and L_a represent, respectively, the gain and absorber section lengths, with:

$$\alpha_m = \left(\frac{1}{L}\right)\ln\left(\frac{1}{\sqrt{R_1 R_2}}\right) \tag{5}$$

where, $\left(L_g + L_a\right) = L$ and R_1, R_2 denote mirror reflectivities.

In the DDE model, G and Q describe the saturable gain and loss introduced by the gain and absorber sections, respectively, and $\kappa < 1$ describes the total roundtrip non-resonant linear intensity losses. Thus, the threshold condition for lasing is given by[12]:

$$\kappa e^{(G-Q)} = 1 \Rightarrow G = Q - \ln(\kappa) \tag{6}$$

Comparing (3) and (4), we find:

$$G_{threshold} = \left(g_{\mathrm{mod}}(J) - \alpha_i\right)L_g \tag{7}$$

$$Q_{threshold} = \left(a_0 + \alpha_i\right)L_a \tag{8}$$

$$\kappa = \sqrt{R_1 R_2} \tag{9}$$

A key feature of the DDE model is its dimensionless formalism, whereby physically measured laser parameters must be scaled appropriately and made dimensionless, before being used as inputs to the model. Thus, in order to enable a direct conversion between measurable static laser quantities and the definitions appearing in [12], transformation relations to relate the saturable gain and absorption (G and Q, respectively) to the corresponding unsaturated parameters (g_0 and q_0, respectively) have been derived to yield:

$$g_0 = \Gamma G \tag{10}$$

$$q_0 = \left(Q/s\right) \tag{11}$$

where,

$$s \equiv \frac{g_q \Gamma_q}{g_g \Gamma_g} = \frac{\left[\partial g_{\mathrm{mod}}(J)/\partial J\right]_{g_{\mathrm{mod}}(J)=0}}{\left[\partial g_{\mathrm{mod}}(J)/\partial J\right]} \tag{12}$$

Further, using the dynamical stability analysis presented in Fig. 5 of [12], it is deduced that a suitable constraint to achieve stable, fundamental mode-locking in terms of g_0 and q_0, yields an expression for the carrier relaxation ratio, Γ, which depends solely on measurable static device parameters defined above in equations (7), (8) and (12):

$$\Gamma = \left(\frac{Q}{mGs}\right) = \frac{\left(a_0 + \alpha_i\right)L_a}{m\left(g_{\mathrm{mod}}(J) - \alpha_i\right)L_g s} \tag{13}$$

where m represents the slope of a line in the g_0 - q_0 plane, chosen to lie within a region corresponding to a desired mode-locking regime. Equations (7) – (13) provide a set of initial conditions that can be used to seed the simulation.

3. MODELING AND EXPERIMENTAL RESULTS

The device simulated in this study - an 8-stack InAs dots-in-a-well (DWELL) passively mode locked laser, was fabricated with a 1-mm absorber section and 7-mm gain section and a 3.5-μm ridge width. The details of device structure, experimental data and results can be found in [9]. The approach used herein follows that discussed in [13] and involves extracting parameters appearing on the right sides of equations (7), (8), (12) and (13) from quantities measured as a function of gain-section current density, wavelength, absorber reverse bias and temperature using the segmented contact method[14, 15]. This enables the parameter space of the system of DDEs given in equations (1)-(3) to be dramatically reduced as follows.

Values of modal gain and unsaturated absorption measured at threshold can be used to calculate $G(\tau = 0)$ and $Q(\tau = 0)$ using equations (7) and (8) as initial conditions for the simulation, given that the onset of lasing occurs at threshold. The corresponding unsaturated parameters g_0 and q_0 can then be obtained from equations (10) and (11). Parameters κ, s and Γ can be extracted from equations (9), (12) and (13), respectively, where the pre-factor m in equation (13) is varied to achieve different mode-locking regimes (fundamental or higher order). The delay parameter (T) was found by scaling the cavity round trip time to absorber recovery timescales measured on a device with a similar epitaxial-structure[16]. Further to the method used in [13], where the spectral filtering coefficient (γ) was judiciously chosen and held constant (and thereby assumed invariant with respect to gain and linewidth enhancement factors), we are now able to estimate this parameter from the measured optical spectrum of the device as the product of the number of cavity modes taking part in the mode-locking process and the cavity inter-mode frequency spacing (T^{-1}). Thus, 7 of the 9 parameters comprising the parameter space of the system of equations (1)-(3) are obtained specific to the device under study at a given set of operating conditions. This leaves just 2 free parameters, namely, the linewidth enhancement factors in the gain and absorber sections, which were kept equal to simplify the analysis.

Table I: Simulation Parameters over bias voltage for device under study at 20 C.

Parameter	0 V	–3 V	–5 V
T	3.23	5.00	6.67
G(0)	3.33	4.18	4.18
Q(0)	2.33	3.20	4.55
α_g	0.1	0.2	0.5
α_q	0.1	0.2	0.5
s	2.68	4.65	6.90
Γ	0.13	0.08	0.08
γ	29.14	39.15	41.10
κ	0.55	0.55	0.55

Table I shows a representative set of parameters used to model the device over bias voltage at 20˚C. The results shown in the following were obtained as follows. The parameter values measured/extracted as discussed above were used as initial conditions for the simulations. Steady state solutions to the system of equations defining the model (equations (1), (2) and (3)) were then found by direct numerical integration over two thousand round trip times to allow transients to settle. By varying the pre-factor m in equation (13), different regimes of mode locked operation were predicted, as seen in the following.

Fig. 1a shows the steady state output of the system of equations in (1)-(3), for the operating condition of T = 20˚C and a 0V absorber bias voltage (simulation parameters listed in the first column of Table I), for various values of the ratio of unsaturated gain to unsaturated absorption.

As seen from Fig. 1a, simulations predict the onset of pulse formation for $(g_0/q_0) \approx (1/8)$. Then, as the ratio of (g_0/q_0) is increased, stable, fundamental mode locking is maintained and the pulses are predicted to become more intense. Next, following a very brief interval of instability in the fundamental mode-locking regime immediately after $(g_0/q_0) = (7/8)$ (characterized by pulses of variable intensity and pulse width), the device switches to stable, second harmonic mode-locking, whereby two pulses are predicted per round trip.

As the ratio (g_0/q_0) is increased past 1, the mode-locking is predicted to degrade, so that the device shows unstable mode-locking initially (with pulses of variable intensity and pulse width), and eventually transitions to chaotic behavior.

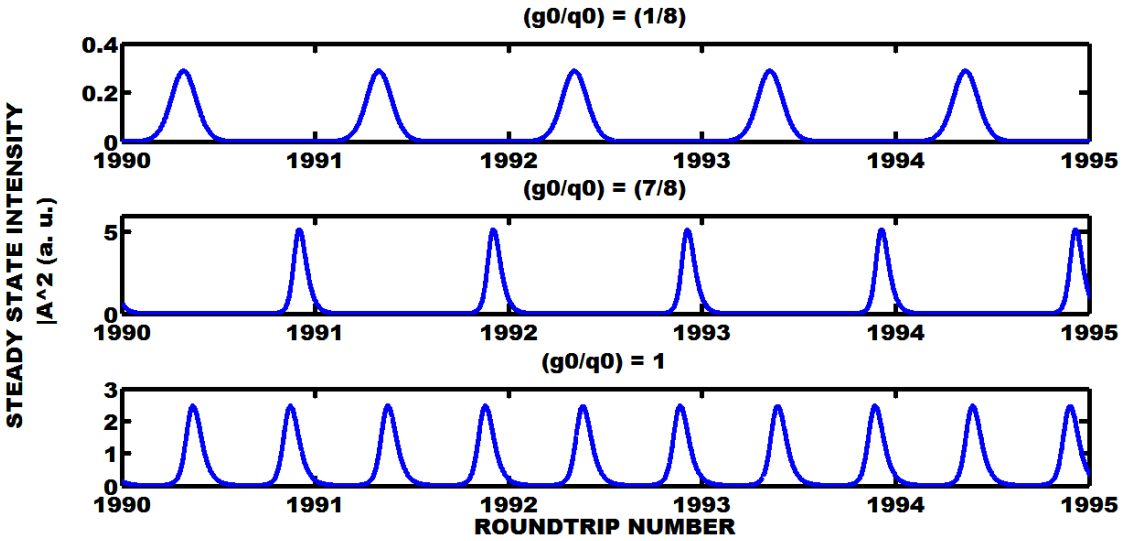

Fig. 1a: Steady state mode locking regimes simulated at 20˚C for 0V absorber bias, i.) fundamental ML for $(g_0/q_0) = (1/8)$, ii.) fundamental ML for $(g_0/q_0) = (7/8)$ and, iii.) 2nd order ML for $(g_0/q_0) = 1$

Thus, the simulation results showed that the device exhibits stable, fundamental mode-locking in the range $(1/8) \leq (g_0/q_0) \leq (7/8)$, past which the device transitions to a pulse-doubling regime. No further higher-order mode-locking regimes were found.

Fig. 1b shows simulation results for an absorber bias voltage of -3V (simulation parameters listed in the second column of Table I). In this case, not only does the model predict a fundamental mode locking regime for $(1/8) \leq (g_0/q_0) \leq (1/2)$, a two-pulse regime for $(1/2) < (g_0/q_0) \leq (7/8)$, but in addition, a three-pulse mode-locked regime of operation for $(7/8) < (g_0/q_0) \leq 1$. Similar to the case for a 0V absorber bias, the mode-locking was predicted to degrade as the ratio (g_0/q_0) was increased past 1, giving way to a chaotic output.

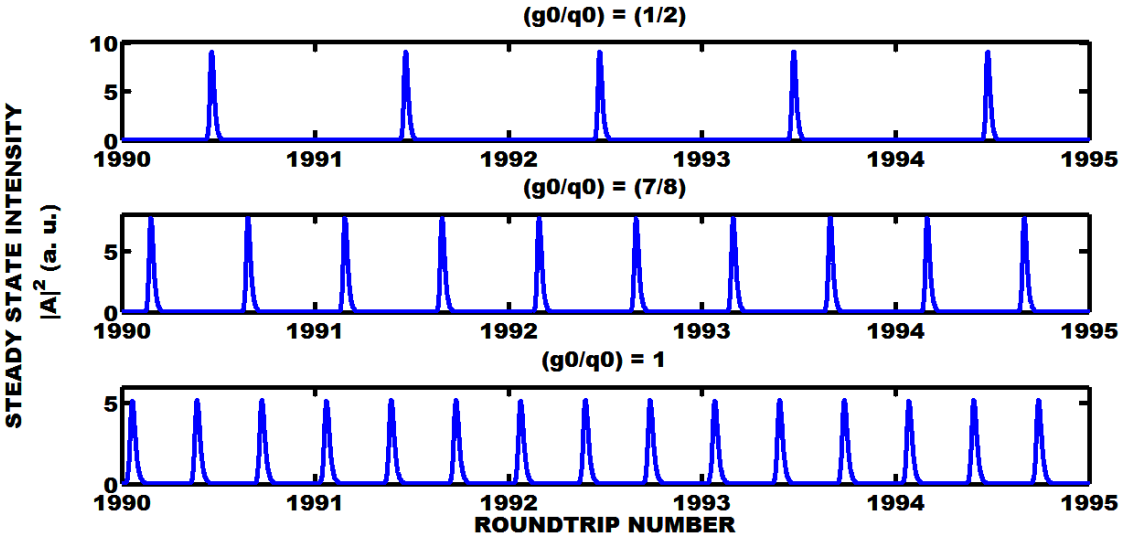

Fig. 1b: Steady state mode locking regimes simulated at 20˚C for -3V absorber bias, i.) fundamental ML for $(g_0/q_0) = (1/2)$, ii.) 2nd order ML for $(g_0/q_0) = (7/8)$ and, iii.) 3rd order ML for $(g_0/q_0) = 1$.

Finally, as seen from Fig. 1c, the nonlinear dynamics of the device output shows an even greater range of operational regimes in its progression from fundamental mode-locking $((1/8) \leq (g_0/q_0) < (5/8))$ to pulse-doubling $((5/8) \leq (g_0/q_0) < (3/4))$ to pulse-tripling $((3/4) \leq (g_0/q_0) < (15/16))$ to pulse-quadrupling $((15/16) \leq (g_0/q_0) \leq 1)$, for an applied absorber bias of -5V (simulation parameters listed in the third column of Table I).

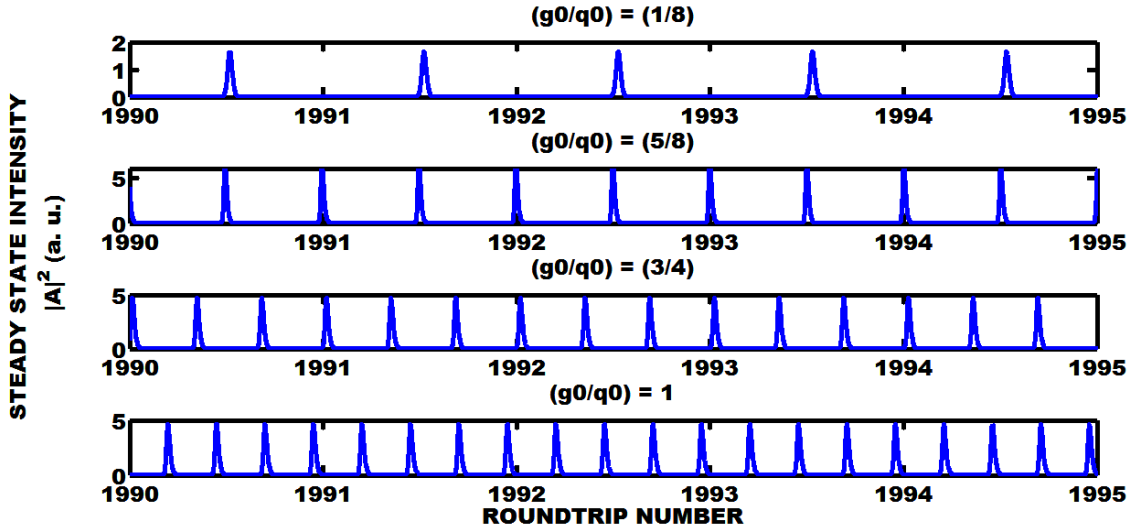

Fig. 1c: Steady state mode locking regimes simulated at 20˚C for -5V absorber bias, i.) fundamental ML for $(g_0/q_0) = (1/8)$, ii.) 2nd order ML for $(g_0/q_0) = (5/8)$, iii.) 3rd order ML for $(g_0/q_0) = (3/4)$, and iv.) 4th order ML for $(g_0/q_0) = 1$.

In this case, as the ratio (g_0/q_0) was increased past 1, an unstable 5-pulse per round trip state was predicted in the range $1 < (g_0/q_0) < 1.3$. For $(g_0/q_0) \geq 1.3$, the output was predicted to be chaotic.
Table II summarizes the results obtained in Fig. 1a-c.

Table II: Predicted ranges of (g_0/q_0) for various mode locking regimes

Absorber Bias (V)	Range of (g_0/q_0)			
	Fundamental Mode-Locking Regime	Pulse-Doubling Regime	Pulse-Tripling Regime	Pulse-Quadrupling Regime
0	$(1/8) \leq (g_0/q_0) \leq (7/8)$	$(7/8) \leq (g_0/q_0) < 1$	*Not Predicted*	*Not Predicted*
-3	$(1/8) \leq (g_0/q_0) \leq (1/2)$	$(1/2) < (g_0/q_0) \leq (7/8)$	$(7/8) < (g_0/q_0) \leq 1$	*Not Predicted*
-5	$(1/8) \leq (g_0/q_0) < (5/8)$	$(5/8) \leq (g_0/q_0) < (3/4)$	$(3/4) \leq (g_0/q_0) < (15/16)$	$(15/16) \leq (g_0/q_0) \leq 1$

The ranges predicted above in Table II for the ratio of dimensionless unsaturated gain (g_0) to dimensionless unsaturated absorption (q_0) can be mapped to externally-controllable biasing parameters (gain section pump current and absorber bias voltage) as follows.
From equation (13) in Section 2,

$$\Gamma = \left(\frac{Q}{mGs}\right) \Rightarrow \left(\frac{1}{m}\right) = \left(\frac{\Gamma Gs}{Q}\right) = \left(\frac{\Gamma G}{Q/s}\right) = \left(\frac{g_0}{q_0}\right) \tag{14}$$

Consider any specific range for the ratio (g_0/q_0), for instance, the range for which pulse-quadrupling is predicted for the -5V bias condition in Table II, so that $(15/16) \leq (g_0/q_0) \leq 1$.
Using equation (14), this range can be expressed as follows:

$$(15/16) \leq (g_0/q_0) \leq 1 \Rightarrow \left(\frac{15}{16}\right) \leq \left(\frac{\Gamma Gs}{Q}\right) \leq 1$$

$$\left(\frac{15Q}{16\Gamma}\right) \leq Gs \leq \left(\frac{Q}{\Gamma}\right) \tag{15}$$

Re-expressing the inequality as shown in (15) yields the range of pump currents at a given absorber bias condition and temperature for which a particular mode locking regime is predicted, given that the saturable gain G and saturation parameter s are both functions of pump current density, extracted directly from modal gain characteristics such as those presented in [9].
Using this approach, the following ranges of pump current are calculated corresponding to the ranges obtained in Table II:

Table III: Predicted ranges of pump current (I_{gain}) for various mode locking regimes

Absorber Bias (V)	Range of I_{gain}			
	Fundamental Mode-Locking Regime	Pulse-Doubling Regime	Pulse-Tripling Regime	Pulse-Quadrupling Regime
0	58mA≤ I_{gain} ≤105mA	105mA<I_{gain} ≤110mA	*Not Predicted*	*Not Predicted*
-3	72mA≤ I_{gain} ≤ 113mA	113mA<I_{gain} ≤136mA	136mA<I_{gain} ≤140mA	*Not Predicted*
-5	84mA≤ I_{gain} ≤140mA	140mA<I_{gain}≤148mA	148mA<I_{gain}≤157mA	157mA<I_{gain}≤160mA

The ranges shown in Table III can be represented as a map showing the approximate regions predicted for each mode-locking regime, as a function of absorber bias vs gain current:

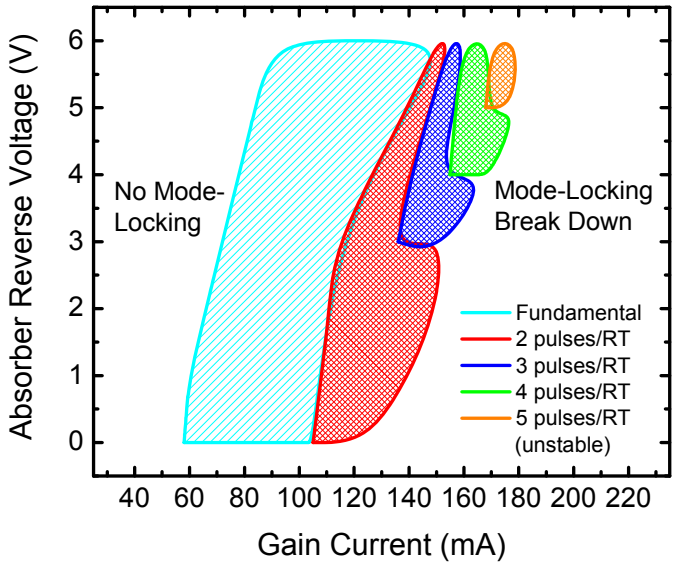

Fig. 2: Predicted regions of fundamental and harmonic mode locking regimes

The practical utility of such a map is evident – the experimenter could simply pick an operating point on the map, lying within a desired regime of operation and bias the device accordingly to achieve a target pulse repetition rate. Following this objective, the device was biased to experimentally achieve the harmonic mode-locking (HML) regimes predicted in Fig. 2. As can be seen clearly from the map, the model predicts a pulse-doubling regime for all bias voltages, and a pulse-tripling regime between an absorber bias of -3 V and -5 V. Several instances of two pulses per round trip were observed experimentally for an applied absorber bias with pump currents above 100 mA, although the second pulse typically appeared as a much weaker "satellite" pulse following the tail of the first (strong) pulse, such as the example seen in the high speed oscilloscope (140 GHz Tektronix DSA 8200 Digital Serial Analyzer) measurement for this device in Fig. 3, recorded for a gain current of 135 mA and absorber bias of - 4.5 V.
Three and four pulses per round trip regimes were not observed for this device. Instead, as the bias voltage was increased for above threshold pump currents, the output pulse shape was observed to exhibit unexpected dynamical trends, such as a reversal of the pulse asymmetry, whereby, the leading edge of the pulse displayed a slower rise time compared to the trailing edge of the pulse, which showed a considerably faster decay.

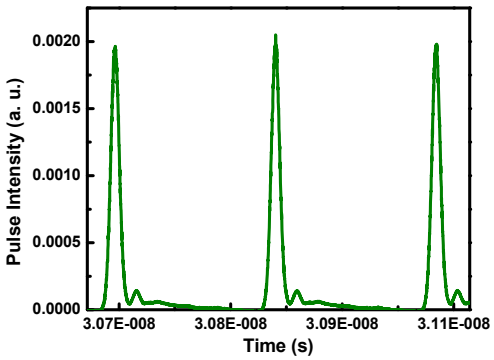

Fig. 3: High Speed Oscilloscope output for -4.5 V absorber bias and 135 mA pump current for Device A. The second pulse is much weaker compared to the first, and appears as a satellite pulse.

However, the broad trends predicted by the map generated from simulation results in Fig. 2 served as a useful guide for other devices with a similar epitaxial structure. Consider, for instance, the following results, obtained with a 6-stack device with a similar epitaxial-structure, 5 μm ridge waveguide and 7 mm gain/1 mm absorber section. The output pulse dynamics were captured using the high speed oscilloscope mentioned above.

The map in Fig. 2 predicts that at low absorber bias voltages, increasing the pump current past 100 mA should result in a transition from fundamental to second harmonic mode locking. For the device under study, this trend is experimentally confirmed in the high speed oscilloscope traces shown in Fig. 4a-c, where for a constant absorber bias voltage of 0 V, increasing the pump current from 75 mA (Fig. 4a) to 100 mA (Fig. 4b) shows the appearance of a second, weaker pulse following the main pulse in each round trip. A further increase of pump current to 125 mA causes the appearance of a two-pulse state, where alternate pulses are identical (Fig. 4c).

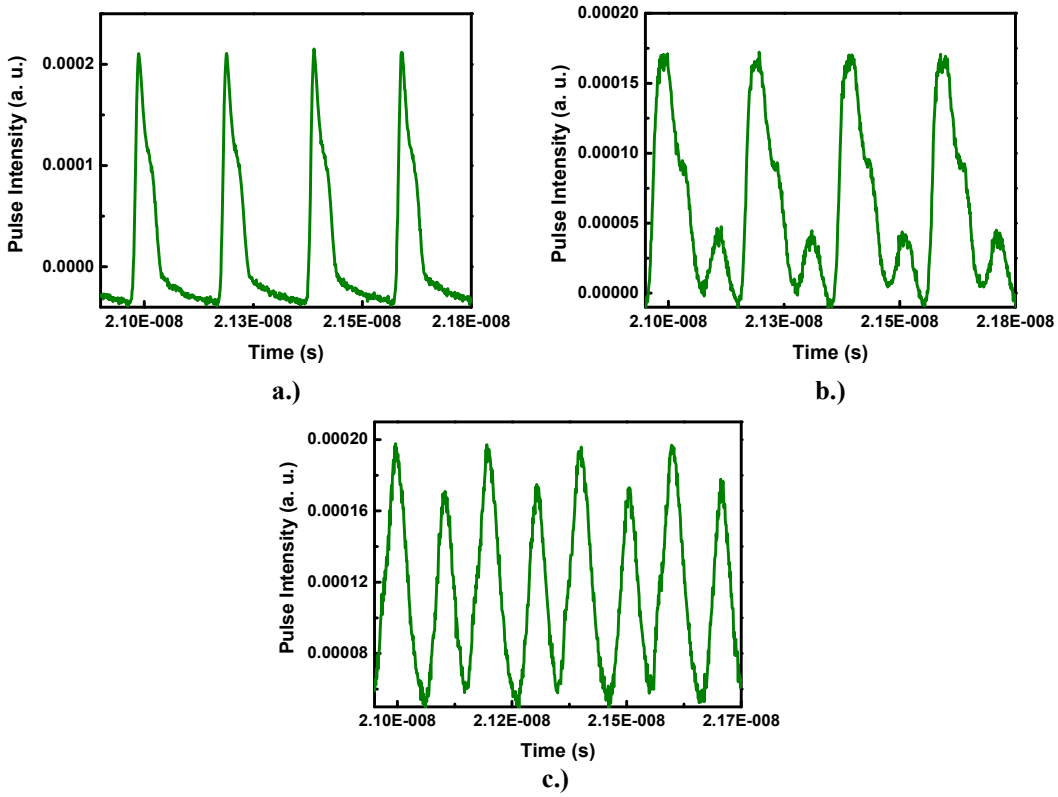

Fig. 4: Output pulse dynamics for a constant absorber bias of 0 V for **a.)** I_{gain} = 75 mA **b.)** I_{gain} = 100 mA, and **c.)** I_{gain} = 125 mA

As is evident from the measured output data, the critical advantage of using this high speed sampling oscilloscope is the ability to capture output pulse train dynamics on the order of nanosecond timescales, as well as the individual pulse shapes comprising the pulse trains.

Further, the map predicts that for currents above 105 mA, if the absorber bias voltage is increased for a fixed value of pump current, the device should produce two pulses per round trip for low and moderate bias voltages ranging from 0 to -3 V, and switch to fundamental mode-locked operation for stronger bias voltages ranging from -4 to -6 V. In this case, the device tested experimentally was identical to the previous device, except for a slightly higher gain-to-absorber length ratio (L_g = 7.2 mm, L_a = 0.8 mm).

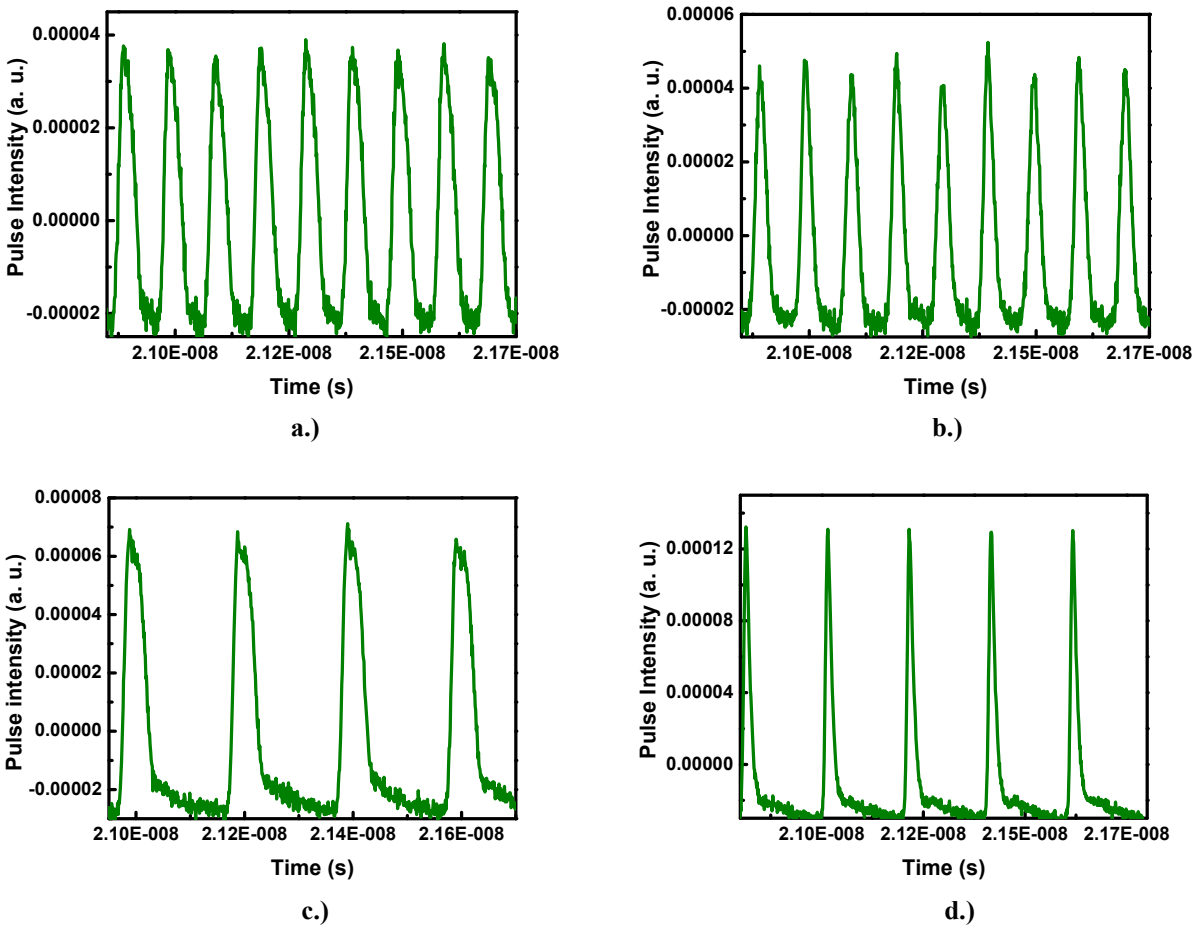

Fig. 5: Output pulse dynamics for a constant gain current of 100 mA, with, **a.)** V_{abs} = 0 V **b.)** V_{abs} = -2 V, and **c.)** V_{abs} = -3 V, and **d.)** V_{abs} = -6 V

Again, as seen from Fig. 5a-d, excellent agreement is seen between the predictions of the map in Fig. 2 and experimental observations for this device. For a pump current of 100 mA and an absorber bias of 0 V, the device is observed to be stably mode-locked, producing two pulses per round trip (Fig. 5a), and this state of second-harmonic mode-locking is maintained as the absorber bias is increased to -1V and -2V (Fig. 5b).

However, keeping the current fixed at 100 mA, when the absorber bias is increased to -3V, the device switches to a state of stable, fundamental mode-locked operation (Fig. 5c). This state of stable, fundamental mode-locking is maintained as the bias voltage on the absorber section is increased, with the best pulse quality achieved at a -6 V absorber bias (Fig. 5d).

And again, despite the numerous experimental observations of dynamical switching from fundamental to second-harmonic mode-locking and vice-versa, higher-order mode-locked states were not observed for these devices.

4. CONCLUSIONS

A nonlinear delay differential equation-based model for passive mode-locking in semiconductor lasers has been shown to offer a robust predictive modeling capability toward achieving higher pulse repetition rates for two-section, passively mode-locked quantum dot lasers. With a parameter space of just nine parameters, seven of which can be experimentally-extracted from measurements on the specific device under study, the model offers a powerful theoretical tool to study the nonlinear dynamics unique to that device. Consequently, the model has been used to first find the regimes of mode-locked operation of a given device wherein the device was predicted to exhibit fundamental or harmonic mode locking, as a function of the dimensionless model parameters. The model parameters were then mapped to externally-controllable parameters (gain section pump current and absorber bias voltage), and the regimes of mode-locked operation were represented on a map, as a function of the said parameters that can be interactively controlled while the device is in operation. Excellent agreement was observed between the predictions of the model and high speed oscilloscope measurements of the output pulse dynamics of fundamental and second-harmonic mode-locking for two devices with a similar epitaxial-layer structure, the first consisting of a 7 mm gain/1 mm absorber section, and the second with a 7.2 mm gain/0.8 mm absorber section (both with a 5 μm ridge waveguide design). The approach not only presents an invaluable guideline toward achieving higher repetition rates without the need to re-engineer the device, but also points toward the highest repetition rates achievable in principle for a given two-section device.

ACKNOWLEDGEMENTS

This work was supported in part by the Air Force Office of Scientific Research under grants FA9550-10-1-0276 and FA9550-10-1-0463, the National Science Foundation under grant ECCS-0903448 and by the Silicon Research Corporation under contract SRC-2009-HJ-2000.
Vassilios Kovanis' work has been supported via the Electromagnetics Air Force Office of Scientific Research Portfolio of Arje Nachman.

REFERENCES

[1] Kuntz, M., Fiol, G., Laemmlin, M., Meuer, C. and Bimberg, D., “High-speed mode-locked quantum-dot lasers and optical amplifiers”, Proc. IEEE 95(9), 1767-1778 (2007).
[2] Carpintero, G., Thompson, M. G., Penty,R. V. and White, I. H., “Low noise performance of passively mode-locked 10-GHz quantum-dot laser diode”, IEEE Photon. Technol. Lett. 21(6), 389-391 (2009).
[3] Schmeckebier, H., Fiol, G., Meuer, C., Arsenijević, D. and Bimberg, D., “Complete pulse characterization of quantum-dot mode-locked lasers suitable for optical communication up to 160 Gbit/s”, Opt. Express, vol. 18(4), 3415-3425 (2010).
[4] Keeler, G. A., Nelson, B. A., Agrawal, D., Debaes, C., Helman, N. C., Bhatnagar, A. and Miller, D. A. B., “The benefits of ultrashort optical pulses in optically interconnected systems”, IEEE J. Sel. Top. Quantum Electron. 9, 477-485 (2003).
[5] Delfyett, P. J., Hartman, D. H. and Ahmad, S. Z., “Optical clock distribution using a mode-locked semiconductor laser diode system”, J. Lightwave Technol. vol. 9(12), 1646-1649 (1991).
[6] Xin, Y.-C., Li, Y., Kovanis, V., Gray, A. L., Zhang, L. and Lester, L. F. , "Reconfigurable Quantum dot Monolithic Multi-Section Passive Mode-Locked lasers", Opt. Express, vol. 15(12), 7623-7633 (2007).
[7] Li, Y., Chiragh, F. L., Xin, Y.-C., Lin, C.-Y., Kim, J., Christodoulou, C. G. and Lester, L. F., "Harmonic mode-locking using the double interval technique in quantum dot lasers," Opt. Express, 18(14), pp. 14637-14643, (2010).
[8] Usechak, N. G., Xin, Y. -C., Lin, C. -Y., Lester, L. F., Kane, D. J. and Kovanis, V., “Modeling and direct electric field measurements of passively mode-locked quantum-dot lasers,” IEEE J. Sel. Top. Quantum Electron. 15, 653–660 (2009).
[9] Crowley, M. T., Murrell, D., Patel, N., Breivik, M., Lin, C. -Y., Li, Y., Fimland, B. O. and Lester, L. F., “Analytical modeling of the temperature performance of monolithic passively mode-locked quantum dot lasers”, IEEE J. Quantum Electron. 47(8), 1059-1068 (2011).

[10] Vladimirov, A. G., Turaev, D. and Kozyreff, G., "Delay differential equations for mode – locked semiconductor lasers", Opt. Lett. 29, 1221-1223 (2004).

[11] Vladimirov, A. G. and Turaev, D., "New model for mode-locking in semiconductor lasers", Radiophys. Quantum Electron. 47, 769-776 (2004).

[12] Vladimirov, A. G. and Turaev, D., "Model for passive mode-locking in semiconductor lasers", Phys. Rev. A 72, 033808-1 – 033808-13 (2005).

[13] Raghunathan, R., Crowley, M. T., Grillot, F., Mukherjee, S. D., Usechak, N. G., Kovanis, V. and Lester, L. F. "Delay differential equation-based modeling of passively mode-locked quantum dot lasers using measured gain and loss spectra", *Physics and Simulation of Optoelectronic Devices XX*, Proc. SPIE 8255, 82551K (2012).

[14] Blood, P., Lewis, G. M., Smowton, P. M., Summers, H., Thomson, J. and Lutti, J. "Characterization of semiconductor laser gain media by the segmented contact method", IEEE J. Sel. Top. Quantum Electron. 9(5), 1275-1282 (2003).

[15] Xin, Y. -C., Li, Y., Martinez, A., Rotter, T. J., Su, H., Zhang, L., Gray, A. L., Luong, S., Sun, K., Zou, Z., Zilko, J., Varangis, P. M. and Lester, L. F., "Optical gain and absorption of quantum dots measured using an alternative segmented contact method", IEEE J. Quantum Electron. 42, 725-732 (2006).

[16] Malins, D. B., Gomez-Iglesias, A., White, S. J., Sibbett, W., Miller, A. and Rafailov, E. U., "Ultrafast electroabsorption dynamics in an InAs quantum dot saturable absorber at 1.3 μm", Appl. Phys. Lett. 89, 171111 (2006).